ADVANCED ENGINEERING MATERIALS

COMMUNICATION

DOI: 10.1002/adem.201500216

Stability of an Amorphous TiCuNi Alloy Subjected to High-Pressure Torsion at Different Temperatures**

By *Dmitry Gunderov,* Viacheslav Slesarenko, Alexander Lukyanov, Anna Churakova, Evgeniy Boltynjuk, Vladinir Pushin, Evgeniy Ubyivovk, Alexander Shelyakov* and *Ruslan Valiev*

The amorphous melt-spun (MS) $Ti_{50}Ni_{25}Cu_{25}$ alloy is subjected to high-pressure torsion (HPT) at temperatures of 20-150 °C. The bright-field (BF) TEM images of the alloy change as a result of HPT processing, the view of the bright-field image depends on the temperature of HPT processing. HPT processing leads to a decrease in the energy of structural relaxation during heating up to 400 °C, in comparison with the initial MS ribbons. The temperature of crystallization of the MS $Ti_{50}Ni_{25}Cu_{25}$ alloy decreases after HPT processing by 40–20 °C (depends on the temperature of HPT processing). In the MS $Ti_{50}Ni_{25}Cu_{25}$ alloy, HPT processing and subsequent annealing produces noticeably finer grains than annealing at 450 °C of the initial MS alloy. Consequently, HPT processing alters the crystallization kinetics of the MS $Ti_{50}Ni_{25}Cu_{25}$ alloy.

Recent studies have shown that severe plastic deformation (SPD) processing can be used not only for grain refinement in metals,[1] but also to produce the amorphous or amorphous-nanocrystalline states, for example, in the case of Nd–Fe–B and Ti–Ni alloys.[2–5] However, there remains a question—are there any differences in the atomic structure of amorphous alloys produced by SPD as compared with amorphous alloys from melt spinning, which allows to obtain thin ribbons by cooling the melt with a high cooling rate (up to $10^6\,K\,s^{-1}$).[6,7]

Plastic deformation in amorphous alloys at relatively low temperatures (<0.5 Tg) proceeds preferably in homogeneously by the formation of shear bands, and this leads to certain structure transformations, associated with the enhanced free volume and crystallization.[7–9] As already noted above, it has been shown recently that SPD processing by HPT can lead to a modification of the amorphous phases.[10–14] For example, in the case of Nd–Fe–B MS amorphous alloys, HPT processing leads to a separation of elements and nanocrystallization of α-Fe-nanocrystals (with a size of ≈20 nm) in the amorphous phase.[10,14] At the same time, HPT processing of the melt-spun amorphous Ti–Ni–Cu alloy does not lead to intensive nanocrystallization.[10,15] In this connection, of great interest are more detailed studies of the evolution of the amorphous structure in this Ti–Ni–Cu alloy during HPT processing and its influence on the alloy's properties. The goal of this work is to perform a complex study of the stability of the amorphous Ti–Ni–Cu alloy subjected to HPT at various temperatures.

1. Materials and Methods

The $Ti_{50}Ni_{25}Cu_{25}$ ingots were re-melted in quartz crucibles under a purified atmosphere of inert gas and ejected onto the

[*] *Prof. D. Gunderov, Dr. A. Lukyanov, A. Churakova, Prof. R. Valiev*
Ufa State Aviation Technical University, 12 K. Marx str., Ufa 450000, Russia
E-mail: dimagun@mail.ru
Dr. V. Slesarenko, E. Boltynjuk, Dr. E. Ubyivovk, Prof. R. Valiev
Saint Petersburg State University, 28 Universitetskiy pr., Saint Petersburg 198504, Russia
Prof. V. Pushin
Ural Division of Russian Academy of Sciences, Institute of Metal Physics, 18 S. Kovalevskaya str., Ekaterinburg 620041, Russia
Prof. A. Shelyakov
National Research Nuclear University MEPhI (Moscow Engineering Physics Institute), 31 Kashirskoe sh., Moscow 115409, Russia

[**] *The authors gratefully acknowledge the financial support of the structural studies provided by the Russian Science Foundation through project No. 14-12-00138. The work was partially supported by the Russian Federal Ministry for Education and Science (through EV Boltynjuk Grant No. 14.B25.31.0017). The scientific investigations were performed at the Research Centre for X-ray Diffraction Studies, Interdisciplinary Resource Centre for Nanotechnology, and the Center for Thermogravimetric and Calorimetric Research of the Research Park of St. Petersburg State University.*

surface of a fast rotating copper wheel at cooling rates around $10^6\,K\,s^{-1}$. The melt-spun ribbons had a thickness of 0.04 mm and a width of about 2 mm. A detailed description of the single-roller melt-spinning technique is given elsewhere.[16,17] SPD processing was carried out by torsion under a pressure of 6 GPa at room temperature (RT) and at temperatures of 50, 100, and 150 °C. The anvils were preliminarily heated to the corresponding temperature, then the sample was placed upon them, and 10 min later HPT processing was started. The HPT processing was performed for up to 10 revolutions at a rotation speed of 1 rev min^{-1}. After the processing was finalized, the samples were removed from the anvils within 2–3 min. As a result, solid samples with a thickness of 0.2–0.3 mm and a diameter of 10 mm were produced from the initial as-spun ribbons. The structure of the samples was investigated by a JEM-2100 transmission electron microscope (TEM) at an accelerating voltage of 200 kV. The foils for the electron microscopy were prepared on the twin jet polishing machine "Tenupol-5" by the standard method at 50 V using a mix of chloric acid (10%) and butanol (90%) as the electrolyte. Foil etching by argon ions was additionally carried out using JEOL ION SLICER EM-09100, at a voltage of 3 kV and an inclination angle of 2°, with the polishing duration about 45 min. Also, the structure was investigated by X-ray diffraction under the Cu radiation employing a Bruker Phaser D2. The disc-shaped samples for TEM and DSC studies were cut out in such a manner that the foil center and the center of the disc corresponded to the point "½ radius of the HPT-sample."

The DSC tests were performed on a Netzsch DSC 204 F1 Phoenix calorimeter; the heating temperature was 520 °C (higher than the crystallization temperature in this alloy) and the typical heating rate was 20 °C min^{-1}.

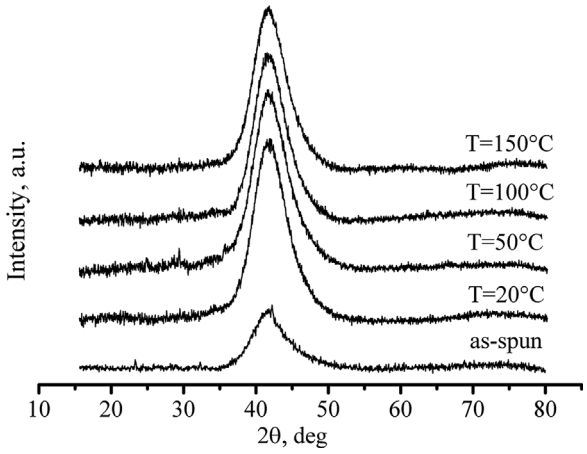

Fig. 1. The XRD patterns of the initial melt-spun $Ti_{50}Ni_{25}Cu_{25}$ ribbon and melt-spun $Ti_{50}Ni_{25}Cu_{25}$ alloy after HPT at different temperatures.

2. Results and Discussion

According to the XRD patterns, the structure of HPT-processed samples as well as the as-spun initial ribbons is amorphous (Figure 1).

The TEM study of the initial melt-spun $Ti_{50}Ni_{25}Cu_{25}$ alloy reveals the amorphous state (Figure 2a). In the selected area electron diffraction (SAED) pattern from an area of 100 nm^2, only the halo of the amorphous phase is observed. Thus, nanocrystals in the observed region are not present, or their

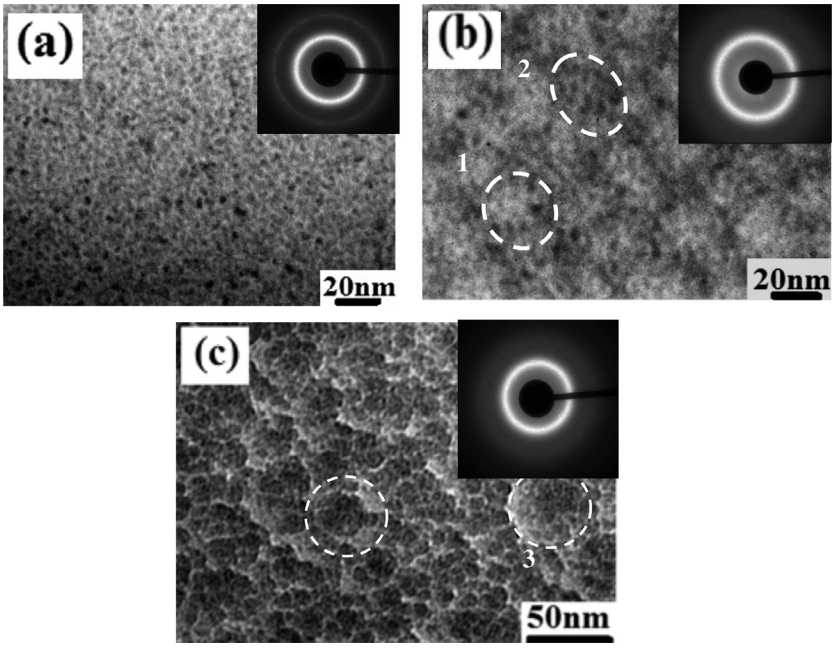

Fig. 2. TEM images of the melt-spun $Ti_{50}Ni_{25}Cu_{25}$ alloy: (a) the initial MS alloy, bright-field image, SAED pattern; (b) after HPT at T = 20 °C, bright-field image, SAED pattern; (c) after HPT at T = 150 °C, bright-field image, SAED pattern; 1, 2–the dashed lines encircle the dark and bright regions ("clusters") in the microstructure after HPT at T = 20 °C; 3–the dashed line encircles the "clusters" after HPT at T = 150 °C.

volume fraction is not significant. The bright-field image exhibits in this case a characteristic "salt-pepper" contrast which is typically observed in amorphous materials.[6]

Figure 2b shows the TEM image of the melt-spun $Ti_{50}Ni_{25}Cu_{25}$ alloy subjected to HPT for up to 10 revolutions at a temperature of $T = 20\,^{\circ}C$. The SAED pattern from an area of $100\,nm^2$ also contains the amorphous halo. In the bright-field image, there can be seen a rather complex picture. Distributed brighter and darker regions with a size of about 20 nm are distinguished in the microstructure.

These regions have the same interior "salt-pepper" structure, the boundaries between them are very blurred, and consequently, these regions are not crystals. Let us call them "bright" and "dark" "clusters."

The microstructures of the MS $Ti_{50}Ni_{25}Cu_{25}$ alloy, subjected to HPT at temperatures of $T = 50\,^{\circ}C$ and $T = 100\,^{\circ}C$, are very similar to the microstructure of the sample processed by HPT at $T = 20^{\circ}C$.

The sample of the MS $Ti_{50}Ni_{25}Cu_{25}$ alloy was also subjected to HPT at a temperature of $T = 150\,^{\circ}C$, the SAED pattern as well contains only the amorphous halo. The microstructure has a number of features observable by TEM (Figure 2c). Dark regions—"clusters" with a size of about 40 nm—become visible in the bright-field image. These "clusters" are separated from each other by thin brighter interfaces, and they also have an internal contrast.

Figure 3 shows the DSC of HPT-processed and as-spun ribbons. The temperatures and energies, obtained by DSC, for the processes of structural relaxation in a temperature range of 20–400 °C and crystallization are shown in Table 1. As a result of HPT processing at 20 °C, the temperature of the crystallization start drops down by about 40 °C in comparison with the initial as-spun amorphous state, and drops down by about 20 °C as a result of HPT processing at 150 °C (Table 1).

In the DSC curve associated with the first heating of the samples, in the temperature range of 120–400 °C there is observed a slight increase of the heat flow corresponding to structural relaxation in the amorphous phases. The evaluation of the energy of structural relaxation during heating up to 400 °C was made in the following way: three successive heatings were conducted in the temperature range of 120–400 °C, and the relaxation energy was determined from the difference in the areas under the curves for the 1st and 3rd heatings (Table 1).

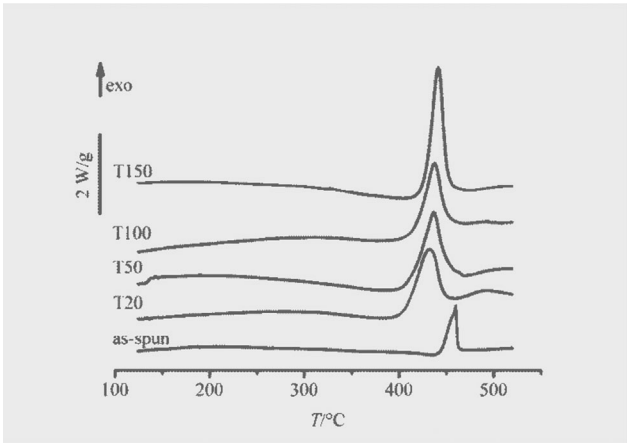

Fig. 3. Calorimetric curves obtained during heating at a heating rate of 20 °C min^{-1} of HPT-processed and as-spun ribbons.

HPT processing leads to a decrease in the energy of structural relaxation in the amorphous phases (in the region of 20–400 °C) in comparison with the initial as-spun ribbons (Table 1). The value of energy remains virtually the same for the samples processed at 20, 50, and 100 °C (Table 1), but for the sample deformed at 150 °C it falls approximately 1.5-fold in comparison with the samples processed by HPT at 20 °C, and approximately 2-fold in comparison with the initial as-spun ribbons. The reduction of the energy of structural relaxation may be associated with a reduced free volume in the amorphous phase.[18]

Analysis also demonstrates that in the MS $Ti_{50}Ni_{25}Cu_{25}$ alloy, HPT processing and subsequent annealing produce markedly finer grains than annealing of the initial MS alloy.[15,19] For instance, the grain size in the MS $Ti_{50}Ni_{25}Cu_{25}$ alloy after annealing at 450 °C for 10 min reaches 1.5 μm (with martensite plate observed within the grains) (Figure 4a), whereas in the MS $Ti_{50}Ni_{25}Cu_{25}$ alloy subjected to HPT and subsequent annealing at 450 °C the grain size is below 100 nm (Figure 4b). Consequently, HPT processing alters the crystallization kinetics of the amorphous phase in the MS $Ti_{50}Ni_{25}Cu_{25}$ alloy.

Thus, according to the DSC data, the TEM bright-field structure of the MS $Ti_{50}Ni_{25}Cu_{25}$ changes in a complex manner after HPT processing. HPT processing also markedly alters the crystallization kinetics of the amorphous phase in

Table 1. Temperatures and energies of structural transformations occurring during heating for as-spun and HPT-processed samples.

Sample	Crystallization peak, [°C]	Crystallization start, [°C]	Crystallization finish, [°C]	Relaxation energy, [J g^{-1}]
As-spun	460	444	463	41
HPT20	432	401	450	37
HPT50	437	408	453	37
HPT100	437	414	455	35
HPT150	441	421	455	24

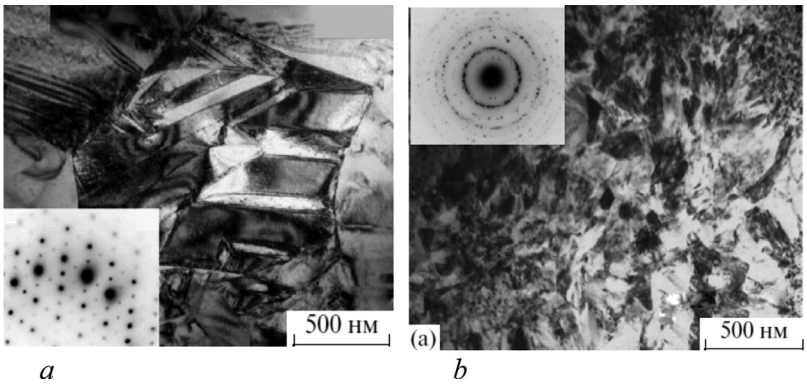

Fig. 4. (a) Bright-field TEM image and the corresponding SAED pattern for the MS $Ti_{50}Ni_{25}Cu_{25}$ alloy after annealing at 450 °C for 10 min; (b) bright-field image and the related SAED pattern (insert) for the MS $Ti_{50}Ni_{25}Cu_{25}$ alloy subjected to HPT ($T = 20$ °C) and subsequent annealing at 450 °C for 10 min.

the MS alloy, which can be accounted for by structural transformations in the material during HPT. The nature of the bright-field contrast in the HPT-processed MS alloy is of particular interest. Of course, the observed contrast depends on the method of the samples (thin foil) preparation, as well as on the mode of TEM recording. However, the observed contrast is different for the samples in different states: for the MS ribbons, for the MS alloy after HPT processing at $T = 20$ °C and at $T = 150$ °C, although the thin foils for all the states were prepared using the same mode. Consequently, the observed contrast reflects the material's structure. According to XRD and SAED patterns, the observed bright-field "clusters" cannot be nanocrystals. Moreover, these "clusters" represent some kind of amorphous structure. What could be the nature of the contrast observed in the bright-field image? This contrast could be the result of the existence in the amorphous phase of regions with a reduced free volume (bright regions, bright boundaries), and with an enhanced free volume (dark regions). The observed picture can be interpreted as a structure of the nanoglass type—nanoscale amorphous "clusters" of the same topology, separated by amorphous boundaries of another topology with an increased free volume.[18,20] The structural feature of the amorphous $Ti_{50}Ni_{25}Cu_{25}$ alloy after HPT processing should be associated with the formation of a high density of shear bands in the amorphous phase during deformation. The width of the shear bands formed in the amorphous phase during deformation was observed at about 10–30 nm,[7] i.e., it is comparable to the size of the "clusters." Single shear bands were not observed in the present study by TEM after HPT processing. This is obviously due to the fact that shear bands are formed in the whole volume of the material and overlap each other during the HPT deformation. It was stated in some studies[11,12] that shear bands are responsible for the enhanced free volume in amorphous alloys after HPT processing. However, in our case it is difficult to explain simultaneously the enhanced free volume and the observed reduction in the energy of structural relaxation in MS alloys after HPT. Perhaps, during the HPT of the MS $Ti_{50}Ni_{25}Cu_{25}$ alloy a redistribution of the free volume takes place, rather than its enhancement. Alternatively, the observed contrast could be accounted for by the different chemical compositions of the «clusters» and their boundaries ("chemical separation") found in some cases in the amorphous phase after plastic deformation.[6,21] In the equilibrium diagram there is no separation of $Ti_{50}Ni_{25}Cu_{25}$ into elements, but the composition fluctuation could manifest itself in the local regions under such extreme treatments as SPD, as was observed earlier during HPT of amorphous MS Nd–Fe–B alloys.[10,13] Nevertheless, this is only one possible explanation, and the nature of such a contrast requires further detailed studies.

3. Conclusions

In summary, it has been shown that:

1) The structure of the MS $Ti_{50}Ni_{25}Cu_{25}$ alloy remains mainly amorphous after HPT processing in the entire temperature range of 20–150 °C.

2) After HPT processing, the TEM bright-field images change considerably and their view depends on the temperature of HPT processing. HPT leads to a decrease of the energy of structural relaxation during heating up to 400 °C, in comparison with the initial as-spun ribbons. The temperature of crystallization start decreases from 445 °C in the initial as-spun ribbons to 400 °C after HPT processing at 20 °C, and to 420 °C after HPT processing at 150 °C.

3) In the MS $Ti_{50}Ni_{25}Cu_{25}$ alloy, HPT processing and subsequent annealing produce much finer grains than the annealing of the initial MS alloy. Consequently, HPT processing alters the crystallization kinetics of the amorphous phase in the MS $Ti_{50}Ni_{25}Cu_{25}$ alloy.

4) All of these observations point to a certain modification of the alloy's amorphous structure during HPT processing, and the kinetics of these changes depends on the temperature of HPT processing. At the same time, the nature of the modification of the amorphous state by SPD processing requires deeper study.

Article first published online: September 11, 2015
Manuscript Revised: June 3, 2015
Manuscript Received: April 28, 2015

[1] R. Z. Valiev, R. K. Islamgaliev, I. V. Alexandrov, *Prog. Mat. Sci.* **2000**, *45*, 103.
[2] N. Boucharat, R. Hebert, H. Roësner, R. Valiev, G. Wilde, *Scripta Mat.* **2005**, *53*, 823.
[3] V. V. Stolyarov, D. V. Gunderov, R. Z. Valiev, A. G. Popov, V. S. Gaviko, A. S. Ermolenko, *JMMM* **1999**, *196-197*, 166.
[4] D. Gunderov, N. Kuranova, A. Lukyanov, V. Makarov, E. Prokofiev, A. Pushin, *Rev. Adv. Mater. Sci.* **2010**, *25*, 58.
[5] J. Huang, Y. Zhu, X. Liao, R. Valiev, *Phyl. Magaz. Let.* **2004**, *84*, 183.
[6] A. L. Greer, in *Rapidly Solidified Alloys*, (Ed: H. H. Liebermann), Marcel Dekker, New York **1993**, p. 269.
[7] Y. Zhang, A. L. Greer, *Appl. Phys. Lett.* **2006**, *89*, 071907.
[8] V. Yu. Zadorozhnyy, A. Inoue, D. V. Louzguine-Luzgin, *Mater. Sci. Eng. A* **2012**, *551*, 82.
[9] Q. S. Zhang, W. Zhang, G. Q. Xie, D. V. Louzguine-Luzgin, A. Inoue, *Acta Mater.* **2010** *58*, 904.
[10] R. Z. Valiev, D. V. Gunderov, A. P. Zhilyaev, A. G. Popov, V. G. Pushin, *J. Metastable Nanocrystal. Mater.* **2004**, *24-25*, 7.
[11] X. D. Wang, Q. P. Cao, J. Z. Jiang, H. Franz, J. Schroers, R. Z. Valiev, Y. Ivanisenko, H. Gleiter, H.-J. Fecht, *Scripta Mater.* **2011**, *64*, 81.
[12] P. Henits, A. Revesz, Z. Kovacs, *J. Mech. Mater.* **2012**, *50*, 81.
[13] W. Li, L. Li, Y. Nan, Z. Xu, X. Zhang, A. G. Popov, D. V. Gunderov, V. V. Stolyarov, *J. Appl. Phys.* **2008**, *104*, 023912.
[14] D. V. Gunderov, V. G. Pushin, R. Z. Valiev, E. Z. Valiev, *Deform. Fracture Mater.* **2006**, *4*, 22. [Rus]
[15] V. G. Pushin, N. N. Kuranova, A. V. Pushin, E. Z. Valiev, N. I. Kourov, A. E. Teplykh, A. N. Uksusnikov, *Phys. Met. Metallogr.* **2012**, *113*, 271.
[16] N. M. Matveeva, V. G. Pushin, A. V. Shelyakov, Y. A. Bykovskii, S. V. Volkova, V. S. Kraposhin, *Phys. Met. Metallogr.* **1997**, *83*, 626.
[17] A. V. Shelyakov, N. M. Matveeva, S. G. Larin, *Shape Memory Alloys: Fundamentals, Modeling and Industrial Applications* (Eds: F. Trochu, V. Brailovski), Canadian Inst. of Mining, Metallurgy and Petrolium, **1999**, p. 295.
[18] H. Gleiter, *MRS Bull.* **2009**, *34*, 456.
[19] A. V. Pushin, V. G. Pushin, A. A. Popov, *Phys. Met. Metallogr.* **2012**, *113*, 283.
[20] H. Gleiter, J. Beilstein, *Nanotechnology* **2013**, *4*, 517.
[21] G. E. Abrosimova, *Physics-Uspekhi* **2011**, *54*, 1227.

